JOURNAL OF CATALYSIS 133, 202–219 (1992)

Pretreatment Chemistry in the Preparation of Silica-Supported Pt, Ru, and Pt–Ru Catalysts: An *in Situ* UV Diffuse Reflectance Study

WEIQING ZOU AND RICHARD D. GONZALEZ[1]

Department of Chemical Engineering, Tulane University, New Orleans, Louisiana 70118

Received May 2, 1991; revised August 16, 1991

Silica-supported metal catalysts were prepared from strongly absorbing $Pt(NH_3)_4(NO_3)_2$ and $Ru(NH_3)_6Cl_3$ precursors at a pH of 9. When supported $[Pt(NH_3)_4]^{2+}$ was directly reduced in H_2 at 400°C, a Pt dispersion of 40% was obtained. Pretreatment in flowing oxygen resulted in a Pt dispersion of 70%. The *in situ* diffuse UV reflectance data suggest that pretreatment in H_2 results in the formation of a mobile $[Pt(NH_3)_2(H)_2]^0$ species. Surface diffusion during reduction results in the agglomeration of Pt particles to form a supported catalyst with a relatively low dispersion. When the decompositon of the Pt precursor is carried out in flowing O_2, a Pt^{2+} precursor with low surface mobility is formed. This results in the formation of a much more highly dispersed Pt catalyst. Studies carried out using $Ru(NH_3)_6Cl_3$ as the metal precursor resulted in very low dispersions when the pretreatment was carried out in O_2. The Ru dispersion was a direct function of the oxidative pretreatment temperature. It was concluded that the mobile surface species consisted of Ru oxides, most likely RuO_4. Reduction in H_2 resulted in the formation of highly dispersed Ru. In addition to diffuse reflectance spectroscopy, surface characterization techniques included TEM, EDXS, and chemisorption.

INTRODUCTION

Recent results suggest that the preferred surface mobility of metal precursors that are weakly adsorbed may lead to the formation of bimetallic clusters that are surface enriched in that metal. Alerasool and coworkers (*1*, *2*) observed that silica-supported Pt–Ru bimetallic clusters prepared from either the corresponding chlorides H_2PtCl_6 and $RuCl_3$ or the amine precursors $Pt(NH_3)_4(NO_3)_2$ and $Ru(NH_3)_6Cl_3$ have surface compositions that are surface enriched in Pt. Miura *et al.* (*3*) showed that this preferential surface enrichment in Pt could be reversed when Pt/SiO_2 was sequentially impregnated with ruthenocene (bis-cyclopentadienyl Ru) followed by reduction in flowing H_2. Augustine and Sachtler (*4*) observed that mixed Pt–Re bimetallic clusters supported on SiO_2 and Al_2O_3 prepared from amine precursors such as $Pt(NH_3)_4(NO_3)_2$ and NH_4ReO_4 can be formed. During reduction, the migration of oxidic Re to zero-valent Pt sites can occur. Because it encounters chemisorbed hydrogen at these sites, reduction of the mobile Re species occurs to form bimetallic particles. Aduriz *et al.* (*5*) reported that Pd–Sn, Sb, Pb, and Ge bimetallic clusters supported on alumina can be prepared from organometallic precursors, such as $(C_4H_4)_4Sn$ and Pd/Al_2O_3, by sequential impregnation. The use of chloride precursors did not lead to the formation of bimetallic clusters. Ru–Rh and Ru–Ir supported on silica prepared from the corresponding chlorides were found to have a homogeneous particle structure with little or no surface enrichment in either metallic component at the surface (*6*).

Calcination in air followed by reduction in H_2 is the normal procedure used in the preparation of supported metal catalysts. However, the chemical implications associated with these pretreatments are not fully understood. The reason for this is the belief

[1] To whom correspondence should be addressed.

0021-9517/92 $3.00

that calcination is performed to burn off and remove impurities from catalysts. Conflicting results have been reported due to different calcination and reduction pretreatments. Studies completed in this laboratory (*2*) show that coimpregnation of $Pt(NH_3)_4(NO_3)_2$ and $Ru(NH_3)_6Cl_3$ in an aqueous silica solution followed by reduction in H_2 leads to the formation of highly dispersed bimetallic particles. The surface composition of these bimetallic particles is enriched in Pt. Pretreatment in O_2 prior to reduction leads to phase separation. The formation of oxidic ruthenium species was suspected as the underlying reason leading to this phase separation.

The purpose of this study represents an effort to understand changes in the anchoring chemistry involved in the pretreatment. In order to explore this chemistry under *in situ* conditions, diffuse UV reflectance spectroscopy was used. Surface compositions of the resulting bimetallic clusters were measured using selective O_2–CO titration techniques while the morphology and individual particle compositions were studied by transmission electron microscopy and energy dispersive X-ray spectroscopy (EDXS).

EXPERIMENTAL

Catalyst preparation. The compounds used as metal precursors in this study were $Pt(NH_3)_4(NO_3)_2$ and $Ru(NH_3)_6Cl_3$ (Strem Chemicals, Newburyport, MA). A dilute solution of HNO_3 (0.1 *N*) was used to wash the support (Cab-O-Sil, M-5, surface area 200 m^2/g, average pore size 14 nm, Cabot Corp., Champaign, IL) to remove traces of alkali metal ions that might have been present on the support. After washing with deionized water, the acid treated Cab-O-Sil was dried in a vacuum desiccator. The silica slurry was prepared by adding the appropriate amount of deionized water to the powder of the acid-treated silica under continuous stirring. The pH of the solution that contained the silica was increased to 9.0 through the dropwise addition of NH_4OH. This pH is higher than that which corresponds to the isoelectric point of silica (*2–4*) but lower than that at which silica begins to dissolve (~10) (*7, 8*). Under these conditions, the negative charge on the silica support is maximized leading to a strong interaction between the support and the cationic precursors in solution (*9*). The total metal loading of the precursor was kept constant at 0.3 mmol of total metal/g of support for both the monometallic and the bimetallic catalysts. The precursors were dissolved in approximately 15 ml of deionized water and then added to the silica slurry. The pH was readjusted to 9.0 and the slurry was covered and stirred for 12 h. The resulting catalyst slurry was filtered and washed with approximately 50 ml of deionized water to remove the weakly adsorbed precursors in addition to chlorides that interfere with the adsorption of CO (*10, 11*). The presence of chloride was shown to inhibit the adsorption of both CO and H_2. Following drying and washing with deionized water, the actual metal loading was measured using ICP. The metal weight loading of the Pt catalyst was 2.68% and for the Ru catalyst it was 1%. The Pt–Ru bimetallic catalyst had a Pt weight loading of 0.98% and a Ru loading of 1.03 wt%. The samples were dried in a vacuum desiccator and either stored or pretreated for future studies.

Pretreatment. Following drying and prior to a chemisorption experiment, the samples were heated to the desired pretreatment/reduction temperature at a heating rate of 10°C/min. The temperature ramp was controlled by a temperature programmer. Tylan electronic flow controllers were used to control the flow rate at 30 ml/min for all gases. Fresh He at a rate of 30 ml/min was used to cool the microreactor that contained the sample. A H_2 reduction temperature of 400°C was used. Reduction time in flowing H_2 was for 3 h followed by a 1-h purge in flowing He at the same reduction temperature. Following each chemisorption experiment the samples were regenerated for the next chemisorption experiment by following identical pretreatment procedures. Except where indicated, treatment in oxygen at temperatures in excess of 150°C was avoided due to possible phase separation and Ru sintering as a result of the formation of volatile ruthenium oxides.

Gas purification. Because trace amounts of oxygen in the ppm range had a marked effect on catalyst morphology at high temperatures, a special effort was made to exclude O_2 from the He, Ar, and H_2 gas streams.

The gases used in this study were purchased from the Linde Co. (Hillside, IL). Argon, helium, oxygen, and hydrogen were ultrahigh purity (UHP) grade (99.999% purity). The carbon monoxide was research grade.

All gases were passed through traps filled with molecular sieves ($\frac{1}{16}$-in. pellets, Linde 13X) in order to remove moisture. These traps were kept at a temperature of −75°C by means of a dry ice/acetone bath. The helium or argon carrier gas was passed through a high gas purifier manufactured by Supelco, Inc. Downstream from the purifier, an additional indicating purifier (OMI-1, Supelco, Inc.) containing a resin and a water reactive solid lithium compound, was installed in order to decrease the oxygen and water content of the carrier gas to less than 10 ppb.

Chemisorption and surface composition measurements. A 150 to 250 mg sample was placed in a pyrex microreactor and subjected to the standard pretreatment. Chemisorption measurements were performed by the dynamic pulse method as described by Sarkany and Gonzalez (*12*). Surface compositions of the bimetallic catalysts were determined by titrating a monolayer of chemisorbed oxygen with CO to a CO_2 end point as described in Ref. (*1, 2*).

In situ diffuse reflectance studies. A UV–VIS spectrophotometer (Perkin–Elmer, Lambda 5) was used for this study. The UV reactor system including an *in situ* cell reactor was designed by the Byron Lambert Co. (Franklin Park, IL) and is shown in Fig. 1. The reactor was made of

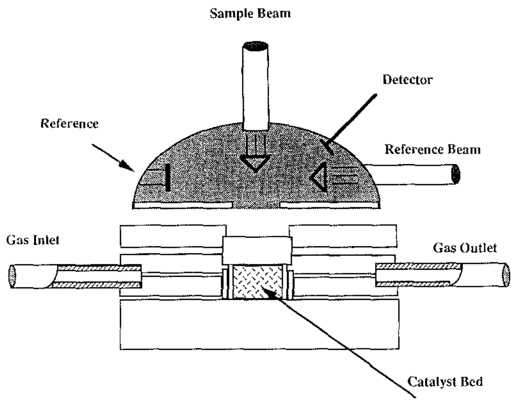

FIG. 1. Diagram of the UV reactor and the integrating sphere.

stainless steel and had a gas inlet and outlet in addition to a throughput for inserting an insulated thermocouple. A specially designed stand equipped with a copper block and a heating element could be used for *in situ* heating up to 500°C. The integrating sphere was externally interfaced with the UV spectrophotometer through the use of fiber optic cables. The reactor was designed so that the integrating sphere could be directly attached to the quartz window of the reactor. A Perkin–Elmer 3600 Data Station was used to collect and process the data. For solution spectra, the instrument was used without the integrating sphere attachment.

Electron microscopy. A small portion of a 5-mg sample was suspended in ethanol. The beaker containing the ethanol suspension was placed in an ultrasonic cleaner and sonicated for a period of 1 min. A drop of this well-mixed suspension was placed on a carbon-coated 300 mesh copper grid. The specimen was placed in the sample holder of the microscope following drying under ambient conditions.

A JEOL 100 CX transmission electron microscope equipped with a LaB_6 crystal was used for this study. It had a maximum magnification of 250 K and a maximum accelerating voltage of 100 KeV. Two specimens were prepared for each sample and as many as 10 spots from different locations on the grid were imaged and recorded in the bright field mode.

Single particle analysis was performed using a VG HB501 scanning transmission electron microscope equipped with a field emission gun. The procedure followed was as described in Ref. (*11*).

RESULTS

Diffuse UV Reflectance Studies

Tetramineplatinum(II) and hexamineruthenium(III) complexes. Mason and Gray (*13*) and Mason (*14*) performed a series of experiments on $[Pt(NH_3)_4]^{2+}$ in different solutions and observed both *d-d* and charge transfer transitions for this complex. The UV spectrum of silica in an aqueous suspension at 25°C is shown in Fig. 2. The intense sharp band centered at 208 nm is in all probability due to excitons that are not able to migrate through the solid. An exciton bound to a defect is simply an alternative way of describing an excited electronic state of the defect (*15*). The intensity of the 208-nm band was considerably smaller for the UV reflectance spectrum of the solid silica. It is rather unfortunate that this silica band centered at 208 nm coincides with the charge transfer band assigned to $NH_3 \rightarrow Pt^{2+}$ for the species $[Pt(NH_3)_4]^{2+}$ (*13, 14*).

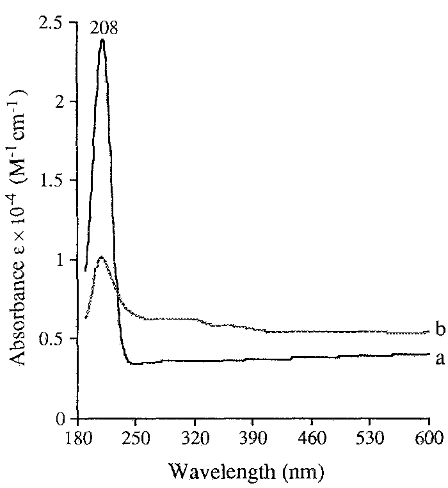

FIG. 2. The UV spectra of high-surface-area silica: (a) in aqueous solution at 25°C; (b) solid in air at 25°C.

Figure 3 shows a comparison of the UV-visible spectra of the tetraamineplatinum(II) and hexamineruthenium(III) complexes in solution (Fig. 3A) to that observed for the corresponding complexes adsorbed on the silica surface (Fig. 3B). The intense feature centered at 225 nm observed for the aqueous solution of $[Pt(NH_3)_4](NO_3)_2$ is a charge transfer transition due to the σ bonds of the NH_3 ligands. A weakly absorbing band centered at 295 nm is due to *d-d* transitions that are common to the structure of square-planar Pt complexes and are consistent with those reported by Mason (*14*). When the $[Pt(NH_3)_4](NO_3)_2$ complex was adsorbed on silica, the charge transfer band was observed to shift to 208 nm. The band centered at 208 nm also includes a contribution due to the defect structure of silica. The band centered at 295 nm due to *d-d* transitions observed in solution was also observed in the spectrum of the adsorbed complex. A second band centered at 240 nm appeared as a shoulder on the large charge transfer band centered at 208 nm (Fig. 3B). This band has been assigned by Mason and Gray (*13*) to *d-d* transitions and in all likelihood was obscured by the intense charge transfer band centered at 225 nm in solution. Because the *d-d* band structure of the $[Pt(NH_3)_4](NO_3)_2$ is essentially retained when the complex is adsorbed on the surface of silica, we conclude that little or no decomposition has occurred on adsorption. It is important to note that the cutoff due to the quartz optical lenses occurs at 190 nm.

The spectrum of the hexamineruthenium(III) complex in aqueous solution is shown in Fig. 3A. Strong charge transfer bands were observed at 200 and 275 nm. A somewhat weaker band was observed at 325 nm. When the complex was adsorbed on silica, the position of the bands was observed to shift to 208 and 267 nm, respectively. The band centered at 325 nm was not observed for the adsorbed complex. The strong absorption band centered at 275 nm has been identified by Hartmann and Buschbeck (*16*) as being due to a charge transfer

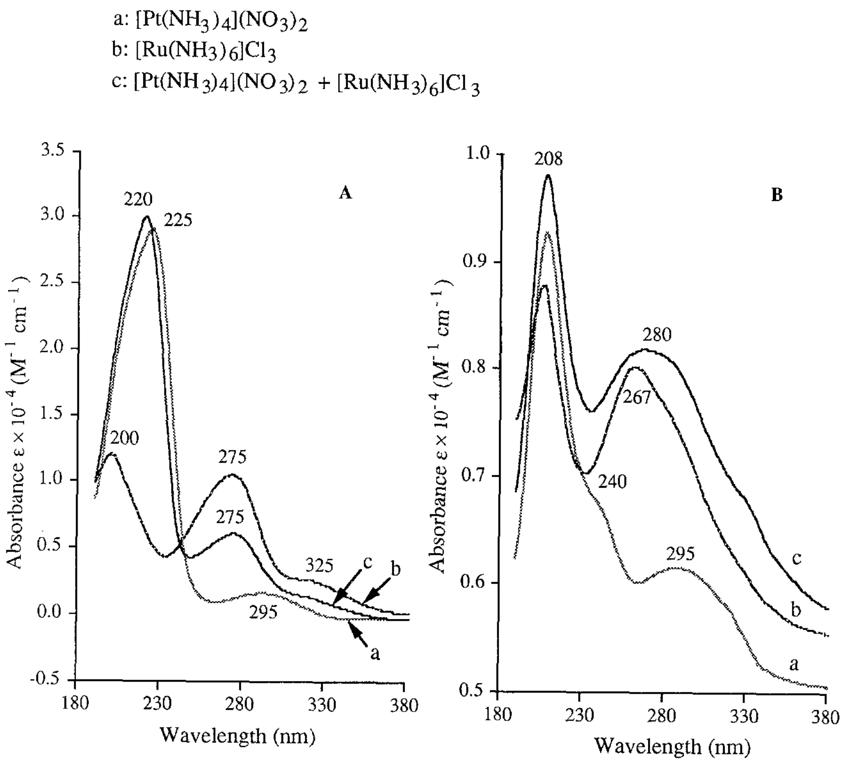

FIG. 3. (A) The UV spectra of different precursors in aqueous solution at 25°C; (B) the UV spectra of fresh samples from different precursors adsorbed on silica.

between the σ bond of NH_3 and the d orbitals of Ru. These authors observed this band at 280 nm. Meyer and Taube (*17*) reported a weak absorption band at 400 nm due to d-d transitions for $[Ru(NH_3)_6]^{2+}$ in solution. In order to assign the absorption features centered at 200 and 325 nm, the spectrum of $[Ru(NH_3)_5Cl]Cl_2$ in aqueous solution at 25°C was compared to that of $[Ru(NH_3)_6]Cl_3$. The results, shown in Fig. 4, suggest that a ligand exchange between an NH_3 ligand and Cl^- has occurred as follows:

$$[Ru(NH_3)_6]^{3+} + Cl^- \rightleftharpoons [Ru(NH_3)_5Cl]^{2+} + NH_3. \quad (1)$$

The spectra shown in Fig. 4 confirm the assignments reported by Hartmann and Buschbeck (*16*). The 200 nm band is assigned to a charge transfer between Cl^- and Ru^{3+} and the band centered at 325 nm is

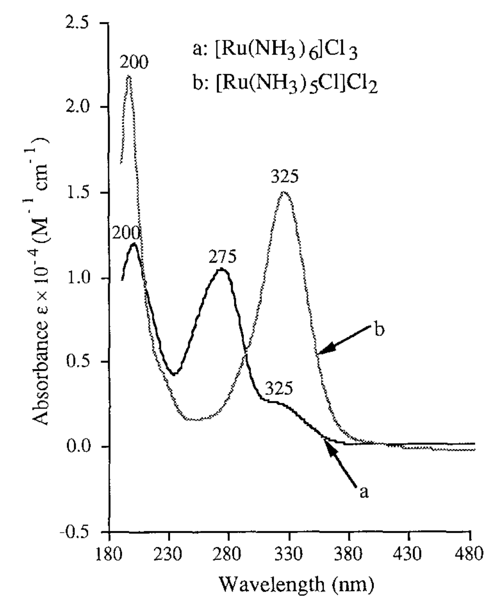

FIG. 4. The UV spectra of Ru precursors in aqueous solution at 25°C.

TABLE 1

UV Band Assignments for $[Pt(NH_3)_4]^{2+}$ and $[Ru(NH_3)_6]^{3+}$ in Aqueous Solution at 25°C

Absorption (nm)	Transition	Proposed species	Reference
198, 225[a]	$NH_3 \rightarrow Pt$ (CT)	$[Pt(NH_3)_4]^{2+}$	*(13, 14)*
290, 295[a]	$d \rightarrow d$	$[Pt(NH_3)_4]^{2+}$	*(13, 14)*
280, 275[a]	$NH_3 \rightarrow Ru$ (CT)	$[Ru(NH_3)_6]^{3+}$	*(16)*
330, 325[a]	$NH_3 \rightarrow Ru$ (CT)	$[Ru(NH_3)_5Cl]^{2+}$	*(16)*
200[a]	$Cl^- \rightarrow Ru$ (CT)	$[Ru(NH_3)_5Cl]^{2+}$	This study

[a] This study.

assigned to an $NH_3 \rightarrow Ru^{3+}$ charge transfer corresponding to $[Ru(NH_3)_5Cl]^{2+}$. The assignments of aqueous Pt and Ru complexes are summarized in Table 1.

In Fig. 3A, spectra obtained for a solution consisting of both tetramineplatinum(II) and hexamineruthenium(III) are consistent with the superposition of the spectra consisting of the individual species. This is also the case for the coadsorption of both complexes onto a silica surface (Fig. 3B).

An *in situ* UV spectrum of $[Pt(NH_3)_4]^{2+}/SiO_2$ in H_2 at different temperatures is shown in Fig. 5A. The ligands released as the result of decomposition in H_2 above 100°C result in the distortion of the original structure. This is evidenced by the complete loss of the *d-d* transition band centered at

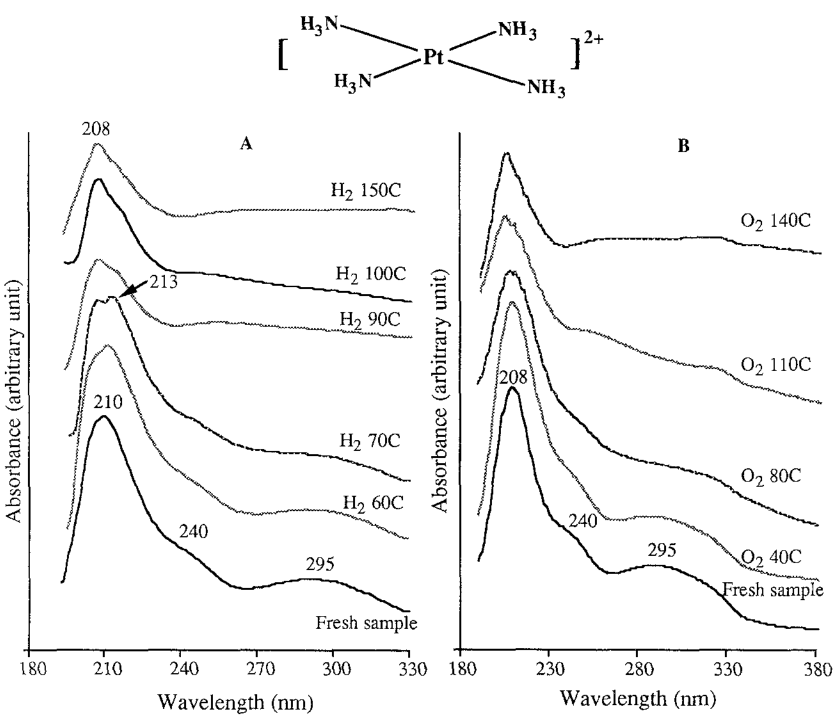

FIG. 5. The UV spectra of $[Pt(NH_3)_4]^{2+}/SiO_2$ at different temperatures: (A) in flowing hydrogen; (B) in flowing oxygen.

TABLE 2

UV Band Assignments for $[Pt(NH_3)_4]^{2+}$ and $[Ru(NH_3)_6]^{3+}$ Supported on Silica

Absorption (nm)	Transition	Proposed species	Reference
208[a]	Exciton	SiO_2	This study
213[a]	$H^- \rightarrow Pt$ (CT)	$[Pt(NH_3)_2(H)_2]^0$	This study
245, 240[a]	$d \rightarrow d$	$[Pt(NH_3)_4]^{2+}$	(*13*)
295[a]	$d \rightarrow d$	$[Pt(NH_3)_4]^{2+}$	This study
267[a]	$NH_3 \rightarrow Ru$ (CT)	$[Ru(NH_3)_6]^{3+}$	This study
400[a]	$(Ru^{II} + Ru^{III}) \rightarrow \pi^*NO$	Mixed (Ru–NO)	This study
360, 370[a]	$Ru^{II} \rightarrow \pi^*NO^-$(CT)	$[Ru^{II}(O_{sil.})_3(NH_3)_x(NO)]$	(*19*)
420[a]	$Ru^{III} \rightarrow \pi^*NO$ (CT)	$[Ru^{III}(O_{sil.})_3(NH_3)_x(NO)]$	This study
540, 540[a]	Not known	Ru red	(*21*)

[a] This study.

295 nm at 90°C. It is important to note the buildup and disappearance of the 213-nm band in the 60–100°C temperature range. Dalla Betta and Boudart (*18*) reported similar results using infrared spectroscopy. A neutral hydride intermediate was suggested as a result of H_2 treatment. The diffuse reflectance spectra reinforce the argument that favors neutral hydride formation and a $H^- \rightarrow Pt$ charge transfer assignment to the UV band observed at 213 nm.

Supporting evidence for the formation of a neutral species is obtained from the oxygen treatment of $[Pt(NH_3)_4]^{2+}/SiO_2$. These results are shown in Figure 5B. It is important to note that the 213 nm was not formed during treatment in oxygen. The UV band assignments of $[Pt(NH_3)_4]^{2+}$ supported on silica are shown in Table 2.

It is well known that Ru complexes are unstable in air. A comparison of the $[Ru(NH_3)_6]^{3+}/SiO_2$ UV spectrum of a fresh sample to that of an aged sample is shown in Fig. 6. Different drying procedures also result in different spectra. Immediately after preparation, a fresh sample of $[Ru(NH_3)_6]^{3+}/SiO_2$ is colorless (Fig. 6a). Following storage in a vacuum desiccator for 2 h a color change to yellow was observed (Fig. 6g). When this sample was exposed to air for 1–2 h the color was observed to change to pink (Fig. 6h).

Treatment of a fresh sample in H_2 at room temperature for a period of 5.5 h resulted in spectrum b (Fig. 6). An intense broadband centered at 400 nm was observed to develop. When the temperature was increased to 40°C in flowing H_2, significant decomposition of the Ru surface complex was observed. The broad feature centered at 400 nm was observed to split into two components centered at 420 and 370 nm (Fig. 6c). Pearce *et al.* (*19*) performed a study in which $[Ru(NH_3)_6]^{3+}$ was supported on X- and Y-type zeolites. They suggested the formation of an amine nitrosyl species in flowing O_2. They observed UV bands centered at 360 and 740 nm following treatment in oxygen at 180°C. The ESCA spectra of these samples as measured by Pedersen and Lunsford (*20*) show that the Ru retains its ionic character following O_2 treatment at 180°C. The most probable oxidation states of Ru are +2 and +3. In accord with Pedersen and Lunsford we assign the bands centered at 420 and 370 nm to ruthenium surface nitrosyls. It is important to note that the 420 nm disappears following reduction in H_2 at 50°C. The band centered at 370 nm disappears at a slightly higher temperature (Fig. 6e). For this reason we assign the feature centered at 420 nm to $Ru^{III} \rightarrow \pi^*NO$ and the band centered at 370 nm to $Ru^{II} \rightarrow \pi^*NO$.

The similarity between the spectra shown in Fig. 6b and that obtained in a vacuum desiccator (Fig. 6g) reinforce the above as-

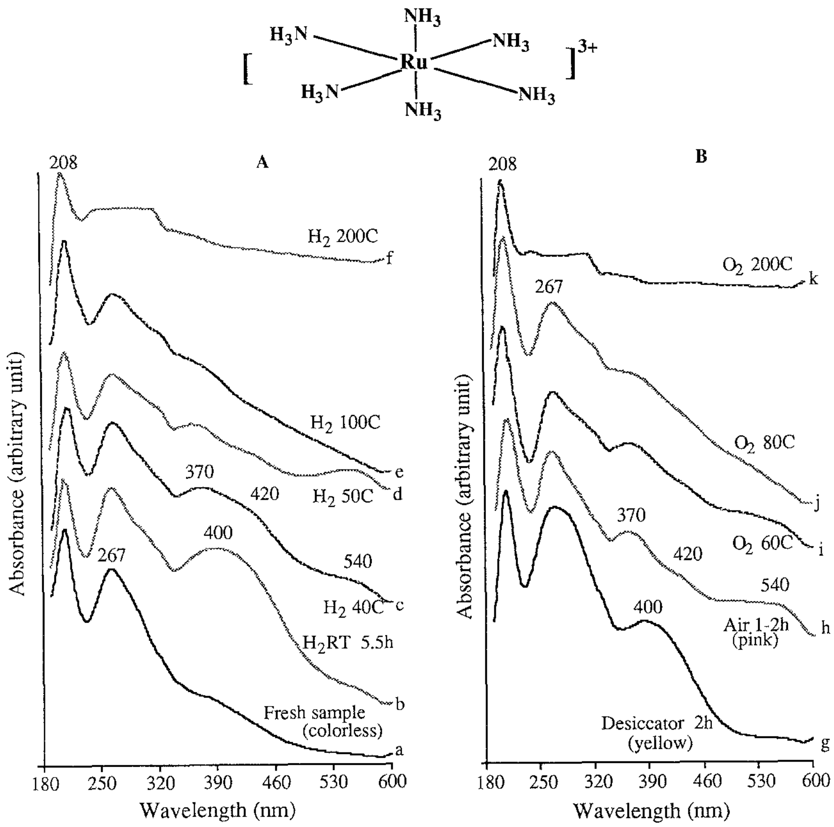

FIG. 6. The UV spectra of $[Ru(NH_3)_6]^{3+}/SiO_2$ at different temperatures: (A) in flowing hydrogen; (B) in flowing oxygen.

signments. When oxygen is excluded the preferred surface configuration appears to be that of a surface nitrosyl. Exposure to air at room temperature results not only in a rapid color change, but also in the decomposition of the surface nitrosyl (Fig. 6h). It is also important to note the appearance of a broadband centered at 540 nm. This band has been identified by Earley and Fealey (*21*) as arising from the species $[Ru^{III}(NH_3)_5\text{–O–}Ru^{IV}(NH_3)_4\text{–O–}Ru^{III}(NH_3)_5]^{6+}$ or "Ru red." It is a species characterized by mixed oxidation states of Ru and is probably responsible for the observed color change. "Ru brown" $[(NH_3)_5Ru\text{–O–}Ru(NH_3)_4\text{–O–}Ru(NH_3)_5]^{7+}$ bands centered at 460 nm (*21*) and oxo-bridged Ru ions $[(NH_3)_5Ru\text{–O–}Ru(NH_3)_5]^{n+}$ with $n = 4, 5$ and UV bands centered at 503 and 616 nm (*22*) were not observed. In a manner similar to that observed for Pt metal precursors, the adsorption of Ru metal precursors on SiO_2 involves little or no perturbation of their structure in solution (Spectrum b in Fig. 3A and 3B). The UV band assignments of $[Ru(NH_3)_6]^{3+}$ precursors supported on silica are summarized in Table 2.

Coimpregnated Pt–Ru precursors. The spectra obtained for the supported Pt–Ru bimetallic clusters corresponding to 50 at.% Ru are shown in Fig. 7. For a freshly prepared sample (Fig. 7a) the broad intense band centered at 280 nm is due to the convolution of the charge transfer band pertaining to $[Ru(NH_3)_6]^{3+}$ centered at 267 nm and the *d-d* transitions of the square-planar complex of $[Pt(NH_3)_4]^{2+}$ centered at 295 nm. It is of interest to note that pretreatment in H_2 at

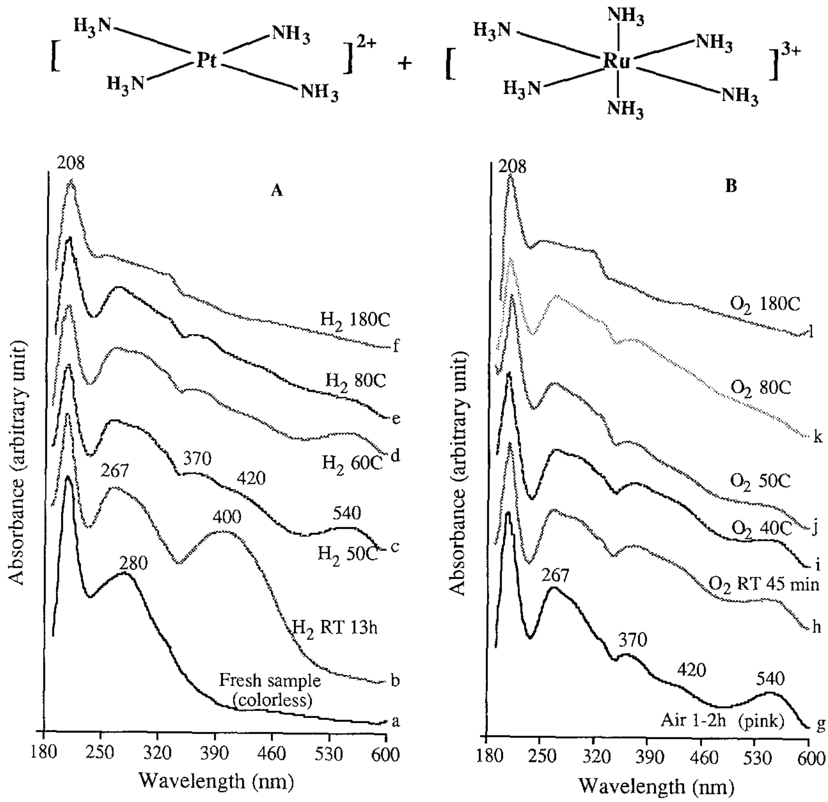

FIG. 7. The UV spectra of ($[Pt(NH_3)_4]^{2+}$ + $[Ru(NH_3)_6]^{3+}$)/SiO_2 at different temperatures: (A) in flowing hydrogen; (B) in flowing oxygen.

room temperature for 13 h leads to the formation of a Ru surface nitrosyl with a prominent feature centered at 400 nm (Fig. 7b). The persistence of the charge transfer band for $[Ru(NH_3)_6]^{3+}$ centered at 267 nm at the expense of the *d-d* transition band centered at 295 nm assigned to the $[Pt(NH_3)_4]^{2+}$ complex, suggests that perhaps the Ru surface complex is the more stable of the two. Heat treatment in flowing H_2 (Fig. 7A) or exposure to oxygen (Fig. 7B) results in the rapid decomposition of both surface complexes.

An analysis of the structure of "Ru red" $[Ru^{III}(NH_3)_5 - O - Ru^{IV}(NH_3)_4 - O - Ru^{III}(NH_3)_5]^{6+}$ shows that because of the bridging oxygen the octahedral (O_h) symmetry is perturbed. This results in the *d*-orbital splitting of the central metal ions Ru^{III} and Ru^{IV}.

Effect of Oxidation Temperature on Metal Dispersion

Ru catalysts. Alerasool and Gonzalez (*2*) reported that the treatment of $[Ru(NH_3)_6]^{3+}$ supported on silica with oxygen prior to reduction results in the formation of large Ru particles. Similar effects have been reported by Lin *et al.* (*23*) and Pearce *et al.* (*19*) for catalysts prepared from the same precursor on alumina and Y zeolites, respectively.

The effect of treating the Ru precursor in O_2 for 30 min prior to reduction in H_2 is shown in Fig. 8. The dispersions shown in Fig. 8 were measured by CO chemisorption and were corrected to include Ru metal loss as a result of the formation of volatile RuO_4. Because the growth of the Ru particles increased as the temperature

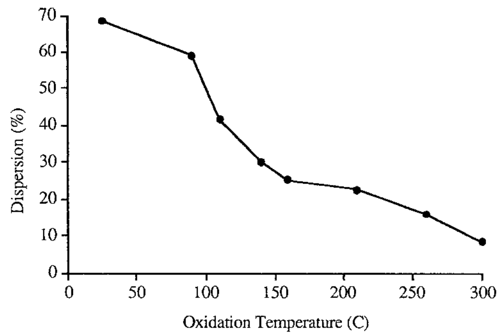

FIG. 8. The dispersion of Ru/SiO_2 catalysts as a function of oxidation temperature.

was increased in flowing O_2, the same sample was used in successive oxidation treatments at the next higher temperature. Results obtained in these sequential oxidation treatments compared favorably to oxidative pretreatments performed starting with fresh samples.

Two oxidation temperatures, 150 and 250°C, were selected for the transmission electron microscopy studies in order to substantiate the particle size distributions obtained using chemisorption. The results are shown in Fig. 9. A large number of particles were observed to fall in the 3–6 nm diameter range. When $[Ru(NH_3)_6]^{3+}$ was reduced in H_2, particles in the 1 nm range were formed. When these particles were treated in O_2 at temperatures as low as 150°C, agglomeration of the Ru particles was observed. This is clearly shown in Figs. 10a–10c. It is of interest to note that in addition to single Ru crystals, polycrystalline aggregates (annular shape) were also observed in the bright field image (Fig. 10b). When the oxidation temperature was increased to 200°C, only randomly oriented single crystal particles were observed (Fig. 10c).

The change in volume of the Ru particles due to the formation of ruthenium oxides and the distance over which the particles migrate across the surface of the support were apparent through the use of TEM methods. The distance between particles

TABLE 3

Average Interparticle Distances as a Function of Oxidation Temperature for Ru/SiO_2 Catalysts

Oxidation temperature (°C)	25	150	250	350
Average interparticle distance (nm)	5.0	9.5	35.0	37.0

was measured for both the reduced sample (i.e., oxidized at 25°C) and the samples treated in oxygen at different temperatures. These results are shown in Table 3. A comparison between dispersions obtained by TEM and by chemisorption is shown in Table 4. Chemisorption results were obtained by performing sequential oxidation experiments starting at a low pretreatment temperature. Some initial oxidation studies were

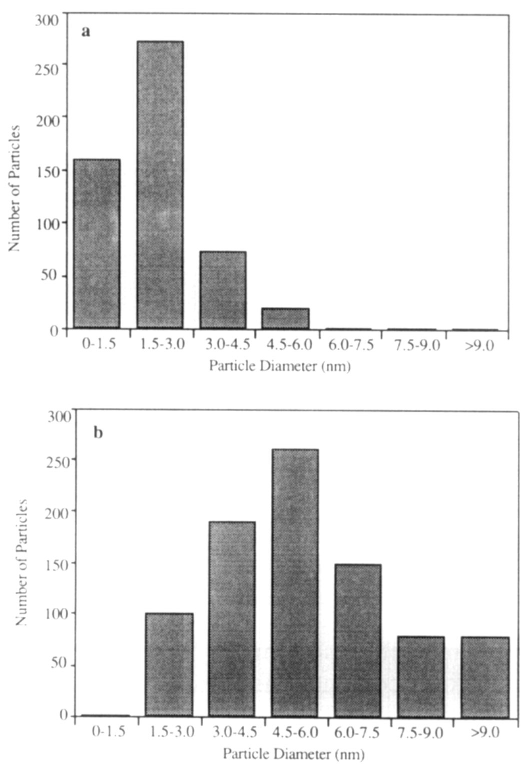

FIG. 9. (a) Particle size distribution of Ru/SiO_2 following O_2 pretreatment at 150°C prior to reduction in H_2 at 400°C. (b) Particle size distribution of Ru/SiO_2 following O_2 pretreatment at 250°C prior to reduction in H_2 at 400°C.

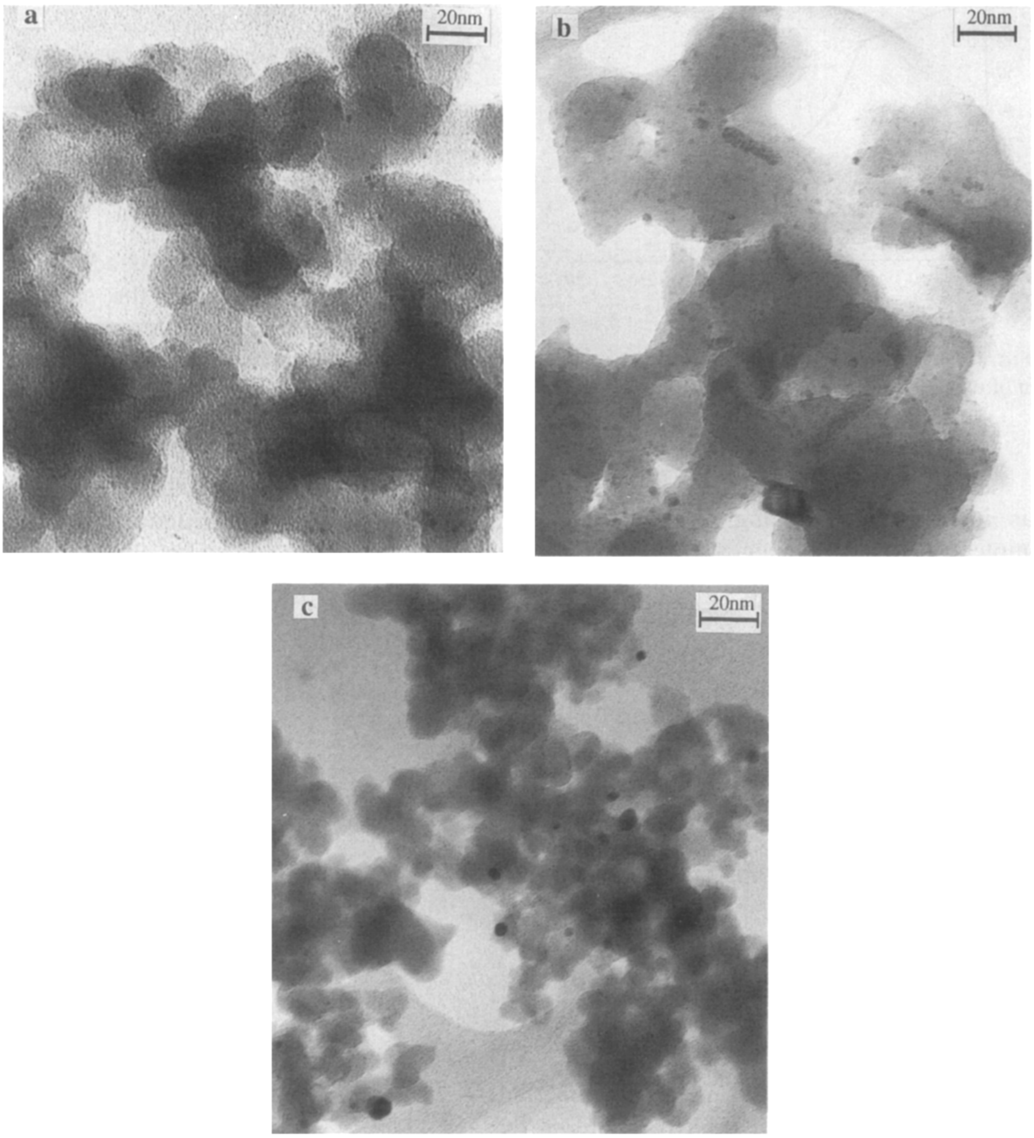

FIG. 10. Transmission electron micrographs of Ru/SiO_2 treated in O_2 at (a) 25°C; (b) 150°C, and (c) 200°C prior to reduction in H_2 at 400°C.

performed on fresh samples for the purpose of making comparisons. These results are also included in Table 4.

The morphological changes observed for Ru due to oxidative treatment at different temperatures are summarized in Fig. 11.

Pt catalysts. The conditions under which the Pt precursor $Pt(NH_3)_4(NO_3)_2$ was pretreated had a significant effect on the dispersion of the resulting Pt/SiO_2 catalysts. This is clearly shown in Figs. 12a–12b. Pretreatment in oxygen at 300°C for 0.5 h following reduction in H_2 at 400C (Fig. 12a) resulted in the formation of particles in the 1.0–1.5 nm range. When $[Pt(NH_3)_4]^{2+}/SiO_2$ was directly reduced in H_2 at 400°C, a large number of particles in excess of 3 nm were observed (Fig. 12b). Particle size distributions

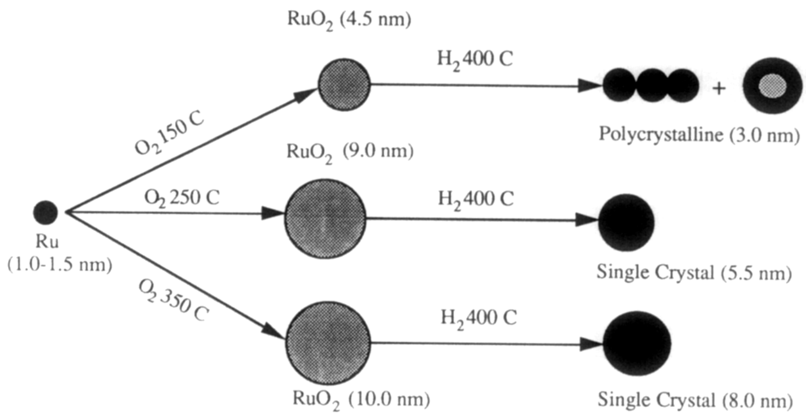

FIG. 11. Morphological changes in Ru as a function of treatment prior to reduction.

are shown in Fig. 13. A comparison between dispersions measured by TEM and by CO and H_2 chemisorption is shown in Table 5. When the results are combined with UV spectra it is concluded that the formation of a Pt neutral hydride species leads to rather poorly dispersed catalysts (40%).

The effect of pretreatment in O_2 at successively higher temperatures is summarized in Fig. 14. The dispersion of the resulting Pt/SiO_2 catalysts is virtually independent of O_2 pretreatment at temperatures up to 300°C. These results were verified using both TEM and chemisorption.

Pt–Ru bimetallic catalysts. The effect of oxidation temperatures on the dispersion of supported Pt–Ru/SiO_2 catalysts is summarized in Fig. 15. A sharp drop in dispersion was observed when the O_2 pretreatment temperature exceeded 175°C. In fact this drop in dispersion paralleled that observed for Ru. In a previous paper Alerasool and Gonzalez (*2*) showed that for a Pt–Ru bimetallic catalyst having a Pt/Ru ratio of 0.5, only bimetallic particles were present. Monometallic particles were not observed. Because of the sharp drop in dispersion observed following pretreatment in O_2 at 200°C

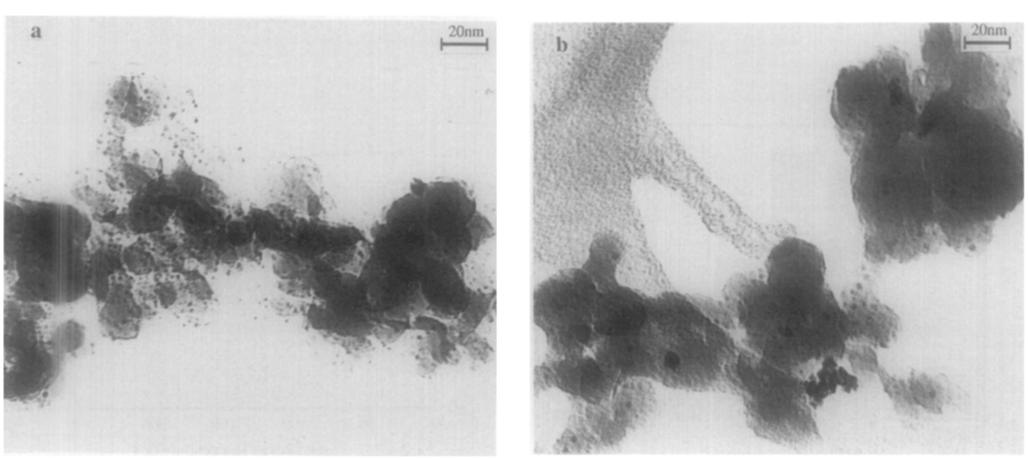

FIG. 12. Transmission electron micrographs of $[Pt(NH_3)_4]^{2+}/SiO_2$ using different pretreatments: (a) O_2, 300°C; H_2, 400°C; (b) H_2, 400°C.

TABLE 4

A Comparison of Dispersions Obtained by CO Chemisorption and by TEM for Ru/SiO_2 Catalysts as a Function of Oxidation Temperature

Oxidation temperature (°C)	Average diameter (nm)	Disp by TEM (%) (100/*d*(nm))	Disp. by CO-chem.	
			Sequential[a]	Initial[b]
25	1.5	66	68	68
150	3.0	33	30	35
250	5.5	18	16	17

[a] Obtained by sequential treatment in O_2 of the same sample.
[b] Obtained by oxidizing a fresh sample at each temperature.

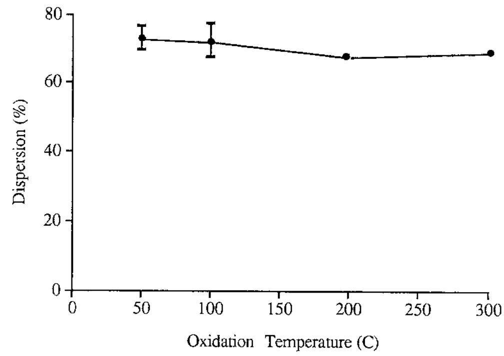

FIG. 14. The dispersion of $[Pt(NH_3)_4]^{2+}/SiO_2$ as a function of oxidation temperature.

prior to reduction, an EDXS analysis of the resulting particles was performed. These results, summarized in Table 6, show that the small particles are primarily bimetallic (somewhat enriched in Ru) while the large particles were essentially pure Ru. There is absolutely no doubt that phase separation has occurred due to treatment in oxygen.

DISCUSSION

Pt catalysts. The diffuse UV results corresponding to the H_2-treated adsorbed $[Pt(NH_3)_4]^{2+}/SiO_2$ precursors is suggestive of the formation of a mobile intermediate Pt surface complex. We formally associate the presence of this surface complex with the $H^- \rightarrow Pt$ charge transfer band centered at 213 nm. The proposed mechanism for the formation of the mobile precursor species can be represented as follows:

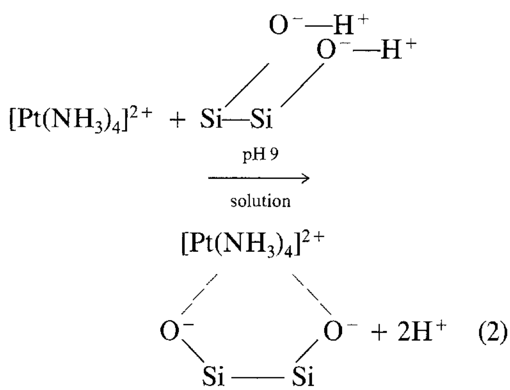

$$2Pt\,(s) + H_2(g) \longrightarrow 2[Pt\text{-}H]\,(s) \quad (3)$$

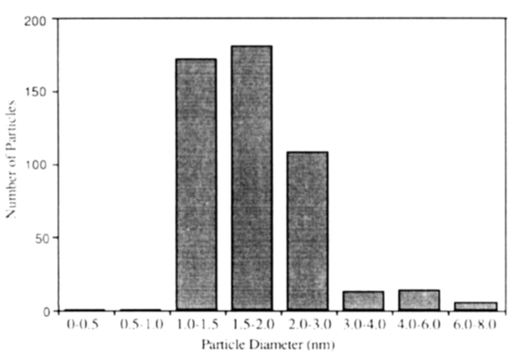

FIG. 13. Particle size distribution of $[Pt(NH_3)_4]^{2+}/SiO_2$ following pretreatment in H_2 at 400°C.

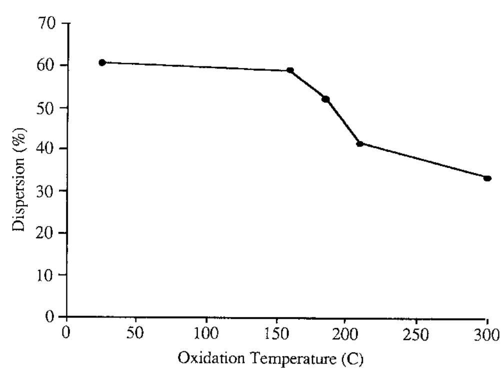

FIG. 15. The dispersion of Pt–Ru bimetallic clusters as a function of oxidation temperature.

TABLE 5

A Comparison of Dispersions Obtained by Chemisorption and by TEM for $[Pt(NH_3)_4]^{2+}/SiO_2$ Catalysts under Different Pretreatments

Catalyst	Pretreatment	D_{CO} (%)	D_{H2} (%)	TEM (100/d(nm))
$[Pt(NH_3)_4]^{2+}/SiO_2$	H_2, 400°C	40	56	45
$[Pt(NH_3)_4]^{2+}/SiO_2$	O_2, 300°C; H_2, 400°C	70	84	70–80
$[Pt(NH_3)_4]^{2+}/SiO_2$	Ar, 300°C; H_2, 400°C	74	85	70–80

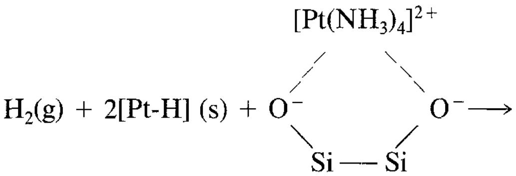

$$2Pt\ (s) + [Pt(NH_3)_2(H)_2]^0(s) + 2NH_3(g) + 2SiOH \quad (4)$$

$$[Pt(NH_3)_2(H)_2]^0\ (s) \rightarrow Pt\ (s) + 2NH_3(g) + H_2(g). \quad (5)$$

Because the 213-nm band was not present when the adsorbed Pt precursor was treated in O_2 it appears that oxygen assists in the rapid decomposition of the adsorbed complex. In oxygen, the adsorbed surface Pt complex was observed to be completely decomposed at 80°C. In H_2, spectral features associated with the surface complex persisted up to about 150°C. There are differences in the surface stability of the adsorbed complex in O_2 on silica and on zeolites. The infrared spectra reported by Dalla Betta and Boudart (18) suggest that when a $[Pt(NH_3)_4]^{2+}$/Y zeolite is heated in oxygen, the complex maintains its structure up to 200°C. The oxidized complex remains ionically bound to the zeolite. Additional data by Gallezot *et al.* (*24*) show that following treatment with O_2 at 300°C most of the Pt is present as Pt^{2+} ions located in the supercages. Treatment in oxygen at 600°C results in the migration of these ions into the sodalite cages. Furthermore, Tzou *et al.* (*25*) reported that the distribution of Pt^{2+} ions between supercages and sodalite cages prior to reduction can be controlled by the calcination temperature in the 360–550°C range.

TABLE 6

Single Particle Analysis for Pt–Ru/SiO_2 Catalysts (Pt/Ru = 0.5)[a]

	D (nm)	% Pt	% Ru	Pt/Ru
1	2	62	38	1.63
2	2	67	33	2.03
3	3	69	31	2.23
4	5	80	20	4.00
5	5	31	69	0.45
6	7	85	15	5.67
7	7	12	88	0.14
8	15	10	90	0.11
9	15	7	93	0.08
10	20	0	100	0.00
11	20	0	100	0.00
12	20	0	100	0.00
13	30	2	98	0.02

[a] Based on atomic mole ratios. The bimetallic catalysts were treated in O_2 at 200°C prior to reduction.

From the above observations, it appears that the decomposition of $[Pt(NH_3)_4]^{2+}$ is more easily accomplished on silica than on a zeolite. This is probably due to structural effects of the support. Arguments concerning the formation and decomposition of PtO_2 have received considerable attention in the literature (*26–28*). PtO_2 is not formed directly from metallic platinum powder by heating in air or in O_2 at temperatures below 600°C. The synthesis of both forms (α and β) of PtO_2 is quite complex. Goncharenko *et al.* (*26*) obtained α-PtO_2 by reacting KNO_3 with K_2PtCl_4 at 400°C for 240 h in a sealed ampule according to

$$KNO_3 + K_2PtCl_4 \rightarrow 3\,KCl + PtO_2 + NOCl. \quad (6)$$

β-PtO_2 was obtained by Tagirov *et al.* (*27*) by decomposing the polymeric product formed in the hydrolysis of potassium trihydroxotrisnitratoplatinate(IV) at 400–500°C. The composition of this polymer can be expressed by the general formula $[Pt(OH)_{4x}(H_2O)_{0.5x}]$, with $x > 4$.

The dissociation temperature of PtO_2 was formulated by Tagirov *et al.* (*27*) as

$$PtO_2\,(s) \rightleftharpoons Pt\,(s) + O_2\,(g) \quad (7)$$

$$\log Po_2,\ \text{Torr} = -11{,}603/T + 15.63\ (595\text{–}655°C). \quad (8)$$

This equation can be used to predict the dissociation temperature of PtO_2. Goncharenko *et al.* (*26*) showed that α-PtO_2 decomposed at 585 ± 10°C, and β-PtO_2 at 620 ± 10°C. From the above discussion it is unlikely that PtO_2 is formed and we feel confident that the decomposition of adsorbed $[Pt(NH_3)_4]^{2+}$ in O_2 should lead directly to the formation of Pt^{2+} according to

$$[Pt(NH_3)_4]^{2+} \rightarrow Pt^{2+} + 4\,NH_3(g) \quad (9)$$

Because the Pt ions formed are positively charged and strongly bound to the surface it is not surprising that the oxidation temperature has little or no effect on the dispersion as shown in Fig. 14. Chen and Schmidt (*28*) observed that Pt sintering occurred following heat treatment in the 500–700°C range. Volatile oxides are formed only above 700°C. Because chlorides were excluded in our method of preparation we rule out Pt surface mobility as a result of the formation of volatile chlorides.

Ru catalysts. The diffuse UV reflectance spectra of the adsorbed $[Ru(NH_3)_6]^{3+}$ complex as a function of the pretreatment variables is suggestive of surface species for which Ru nitrosyls appear to play a very important role. At the very high pH used for the adsorption of the Ru precursor, $[Ru(NH_3)_6]^{3+}$ is very strongly adsorbed on the surface of silica and has a low surface mobility. In the presence of oxygen, Ru is rapidly oxidized to mobile surface species at temperatures as low as 150°C. In order to explain the UV results we suggest the following chemistry, which is consistent with the formation of surface nitrosyls,

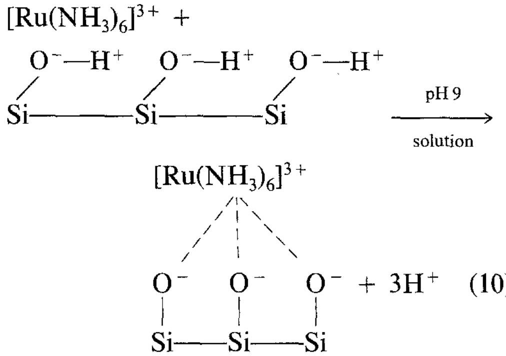

(10)

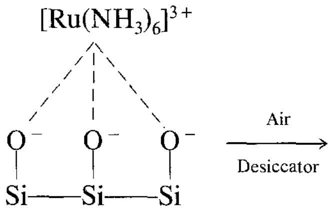

$$[Ru^N(O_{sil.})_3(NH_3)_x(NO)] + Y\,NH_3. \quad (11)$$

In the above representation of the proposed surface complex, N is the oxidation state of Ru. When the catalyst is stored in a vacuum desiccator for extended periods of time and air is excluded, the oxidation state is close to +2 as evidenced by the absorption band centered at 370 nm. The high Ru dispersion obtained following pretreatment in H_2 is probably due to the fact that Ru^{2+} ions are strongly bound to the surface of silica. The poorly dispersed Ru catalysts obtained following pretreatment in O_2 are probably due to the formation of mobile ruthenium oxides, which lead to the agglomeration of Ru particles. Based on free energies of formation (Appendix), it is likely that the oxidic species that leads to sintering is RuO_4.

Exposure of $[Ru(NH_3)_6]^{3+}$ dried in the vacuum desiccator to air at room temperature resulted in the disappearance of the

$[Ru^{II}(NO)^+]$ UV band centered at 400 nm (note Figs. 6h–6i). The ruthenium surface complex retains several of its NH_3 ligands at temperatures up to 170°C. This is evidenced by the persistence of the charge transfer band centered at 267 nm in flowing H_2 (Fig. 6).

Some surface complexes involving mixed oxidation states of Ru such as ruthenium red were undoubtedly present. Because these states have been shown to lead to poorly dispersed Ru particles (30) the band centered at 540 nm due to Ru red was carefully monitored. The band was easily eliminated by exposing the adsorbed Ru precursor to O_2 at 80C (Fig. 6j) or by treatment in H_2 at 100°C (Fig. 6e). Perhaps polymerization of these mixed oxidation states may be partially responsible for the rather poor Ru dispersions obtained following treatment in air. However, we feel that we have presented overwhelming evidence for Ru particle growth through the formation and the rather high surface mobility of Ru oxides.

RuO_2 can be prepared by heating metallic Ruthenium in a stream of air. Under oxidizing conditions, volatilization was observed to take place with the formation of RuO_3 (gas) and RuO_4 (gas) in the vapor phase. Tagirov *et al.* (*31*) investigated the properties of RuO_2 and concluded that

$$RuO_2\,(s) \rightleftharpoons Ru\,(s) + O_2\,(g) \qquad (12)$$

$$\text{Log}\, Po_2,\ \text{Torr} = -15{,}000/T + 10.85 \quad (717\text{–}917^\circ\text{C}). \qquad (13)$$

The decomposition temperature for the Ru oxides are 1127 and 25°C for RuO_2 and RuO_4, respectively (*32*). For this reason, the end product for the oxidation of Ru complexes should be RuO_2. This observation was confirmed by Pearce *et al.* (*19*) using X-ray diffraction methods.

It is of interest to discuss the findings shown in Fig. 10. Reduction in H_2 at 400°C following exposure to O_2 at 25°C resulted in the formation of small highly dispersed Ru particles (Fig. 10a). Heat treatment in O_2 at 200°C prior to reduction resulted in the formation of large very poorly dispersed Ru particles (Fig. 10c). However, pretreatment in O_2 at intermediate temperatures (Fig. 10b) resulted in the formation of polycrystalline aggregates in which donut-shaped agglomerates were clearly observed. We surmise that the formation of oxidic particles is accompanied by a substantial volumetric expansion. Following reduction, the outline corresponding to the expanded oxide particle remains imprinted on the silica and is clearly visible. For several particles that are close together, migration of the resulting oxidic particles in a radial direction occurs leading to the formation of an annular ring. It is this mobility that leads to phase separation when Pt–Ru/SiO_2 bimetallic particles are treated in O_2 at 200°C (see Table 6). Volatile Ru oxides that diffuse away from the bimetallic particles are formed.

CONCLUSIONS

The following conclusions emerge as a result of this study:

(*1*) *$[Pt(NH_3)_4]^{2+}/SiO_2$ catalysts.* The adsorption of $[Pt(NH_3)_4]^{2+}$ complexes on silica occurs without decomposition. The presence of oxygen assists in the decomposition of the adsorbed complex. A neutral hydride $[Pt(NH_3)_2(H)_2]^0$ is formed in a stream of hydrogen in the 60–100°C range. This intermediate, which has a UV absorption band centered at 213 nm, is proposed as a mobile surface species. The decomposition of $[Pt(NH_3)_4]^{2+}$ is more easily accomplished on silica than in a zeolite. The decomposition of $[Pt(NH_3)_4]^{2+}$ in oxygen leads to the direct formation of Pt^{2+}, which is strongly bound to the surface of the support. The oxidation temperature has little or no effect on the dispersion of Pt/SiO_2.

(*2*) *$[Ru(NH_3)_6]^{3+}/SiO_2$ catalysts.* The adsorption of $[Ru(NH_3)_6]^{3+}$ complexes on silica involves little or no perturbation of their structure in solution. These catalysts are easily oxidized in air and show a strong interaction between the Ru precursor and the support. Two oxidation states of the precursor have been observed. Ruthenium nitrosyls disappear following treatment in hydrogen and oxygen below 100°C. The agglomeration of the Ru particles was observed in oxygen at temperatures as low as 150°C. Both single crystals of Ru and polycrystalline aggregates were observed. Ru dispersions were observed to decrease with increasing oxidation temperature.

(3) Pt–Ru/SiO$_2$ bimetallic catalysts. The Ru surface complex is more stable than the Pt surface complex. In H_2, the more mobile Pt phase can diffuse across the support to reduced Ru surface sites where it is reduced in the presence of chemisorbed H_2. Treatment in flowing O_2 at temperatures above 200°C results in phase separation.

APPENDIX

A. Properties of the Stable Oxides of Some Noble Metals

Oxide	State	Dissociation temperature (°C)	Optical properties	Symmetry and structure	Reference
α-PtO_2	Solid	585 ± 10		Hexagonal	*(26, 27)*
β-PtO_2	Solid	620 ± 10		Orthorhombic, Distorted rutile	*(26, 27)*
Pt_3O_4	Solid	700		Cubic	*(26)*
PtO	Solid	500			*(33)*
RuO_2	Solid	>800 (vacuum)	Black, gray	Tetragonal	
		1400		Rutile	*(26, 31, 32)*
RuO_4	Solid	25	Golden yellow		
			Yellow		*(32)*

B. Free Energy (ΔG^0_{25}, kcal/mole) of Platinum Oxides

Oxide	State	Ref. *(32)*	Ref. *(33)*	Ref. *(34)*
PtO	Gas	87.59		
PtO	Solid	−21.03		−11
PtO_2	Gas	22.41	40.1	
PtO_2	Solid	−36.92 ± 10		−20
Pt_3O_4	Solid	−75.94 ± 23.88	−50.92	−14.3

C. Free Energy (ΔG^0_{25}, kcal/mole) of Ruthenium Oxides

Oxide	State	Ref. *(32)*	Ref. *(33)*	Ref. *(34)*
RuO	Gas	81.76		
RuO_2	Gas			38
RuO_2	Solid	−40.87		−44
RuO_3	Gas	−38.44		
RuO_3	Solid			−42
RuO_4	Gas	−64.82		−33
RuO_4	Solid	−67.23	−80.95	−32

ACKNOWLEDGMENTS

The authors acknowledge support from the U.S. Department of Energy (Grant DOEFG02-86ER-1351) for this research. We also acknowledge the Electron Microscopy Facility at the University of Illinois at Chicago for the use of their facility. Finally we thank Dr. Bradley from The Allied Signal Corporation for making their microscope available to us and for assistance in the performance of the AEM analysis.

REFERENCES

1. Alerasool, S., Boecker, D., Rejai, B., Gonzalez, R. D., del Angel, G., Azomosa, M., and Gomez, R., *Langmuir* **4,** 1083 (1988).
2. Alerasool, S., and Gonzalez, R. D., *J. Catal.* **124,** 204 (1990).
3. Miura, H., Tagushi, K., Sugiyama, K., Matsuda, T., and Gonzalez, R. D., *J. Catal.* **124,** 194 (1990).
4. Augustine, S. M., and Sachtler, W. M. H., *J. Catal.* **116,** 184 (1989).
5. Aduriz, H. R., Bodnariuk, P., Coq, B., and Figueras, F., *J. Catal.* **119,** 97 (1989).
6. Miura, H., Feng, S. S., Saymeh, R., and Gonzalez, R. D., *ACS Symp. Ser.* **288** (25), 294 (1985).
7. Brunelle, J. P., *Pure Appl. Chem.* **50,** 1211 (1978).
8. Subramanian, S., Noh, J. S., and Schwarz, J. A., *J. Catal.* **114,** 433 (1988).
9. Benesi, H. A., and Curtis, R. M., *J. Catal.* **10,** 328 (1968).

10. Narita, T., Miura, H., Ohira, M., Sugiyama, T., Matsuda, T., and Gonzalez, R. D., *J. Catal.* **103,** 492 (1987).
11. Narita, T., Miura, H., Ohira, M., Sugiyama, T., Matsuda, T., and Gonzalez, R. D., *J. Appl. Catal.* **32,** 185 (1987).
12. Sarkany, J., and Gonzalez, R. D., *J. Catal.* **76,** 75 (1982).
13. Mason, W. R., and Gray, H. B., *J. Am. Chem. Soc.* **90,** 5721 (1968).
14. Mason, W. R., *Inorg. Chem.* **25,** 2925 (1986).
15. Knox, R. S., *Solid State Phys.* **5,** 1 (1963).
16. Hartmann, H., and Buschbeck, C., *Z. Phys. Chem.* **11,** 120 (1957).
17. Meyer, T., and Taube, H., *Inorg. Chem.* **7,** 2369 (1968).
18. Dalla Betta, R. A., and Boudart, M., *in* "Proceedings, 5th International Congress on Catalysis, Palm Beach, 1972" (J. W. Hightower, Ed.), p. 1329. North-Holland, Amsterdam, 1973.
19. Pearce, J. R., Gustafson, B. L., and Lunsford, J. H., *Inorg. Chem.* **20,** 2957 (1981).
20. Pederson, L. A., and Lunsford, J. H., *J. Catal.* **61,** 39 (1980).
21. Early, J. E., and Fealey, T., *Inorg. Chem.* **12,** 323 (1973).
22. Fink, M. E., Magde, D., Sexton, D., and Ford, P. C., *Inorg. Chem.* **23,** 1238 (1984).
23. Lin, Z. Z., Okuhara, T., and Misono, M., *J. Phys. Chem.* **92,** 723 (1988).
24. Gallezot, P., Alarcon-Diaz, A., Dalmon, J. A., Renouprez, A. J., and Imelik, B., *J. Catal.* **39,** 334 (1975).
25. Tzou, M. S., Teo, B. K., and Sachtler, W. M. H., *J. Catal.* **113,** 220 (1988).
26. Goncharenko, G. I., Lazarev, V. B., and Shaplygin, I. S., *Russ. J. Inorg. Chem.* **30** (12), 1723 (1985).
27. Tagirov, V. K., Chizhikov, D. M., Kazenas, E. K., and Shubochkin, L. K., *Russ. J. Inorg. Chem.* **21** (8), 1411 (1976).
28. Chen, M., and Schmidt, L. D., *J. Catal.* **55,** 348 (1978).
29. Schreiner, A. F., Lin, S. W., Hauser, P. J., Hopcus, E. A., Hamm, D. J., and Gunter, J., *Inorg. Chem.* **11,** 880 (1972).
30. Mieth, J. A., and Schwarz, J. A., *J. Catal.* **118,** 203 (1989).
31. Tagirov, V. K., Chizhikov, D. M., Kazenas, E. K., and Shubochkin, L. K., *Russ. J. Inorg. Chem.* **20** (8), 1133 (1975).
32. Samsonov, G. V., "The Oxide Handbook," pp. 26–50. IFI/Plenum, New York, 1982. [Translated from Russian by R. K. Johnston]
33. R. C. Weast, Ed., "Handbook of Chemistry and Physics," p.D(48–82). CRC, Boca Raton, FL, 1984.
34. Karapet'yants, M. Kh., and Karapet'yants, M. L., "Handbook of Thermodynamic Constants of Inorganic and Organic Compounds," pp. 214–223. Wiley, New York, 1968.